Tilden Lecture: Shining light on metal catalysts

John Evans

Department of Chemistry, University of Southampton, Southampton, UK SO17 1BJ

CHEMICAL SOCIETY REVIEWS

X-Ray absorption spectroscopy can provide local structural information about the reaction centres in metal catalysts. Developments in this technique are illustrated with the chemistry of oxide supported metals *e.g.* $Rh(CO)_2$/titania and by studies on some homogeneous catalysts (rhodium-catalysed carbonylation and nickel catalysts for alkene catenation). Energy dispersive EXAFS promises the opportunity to probe the structures of short-lived reaction intermediates.

1 Introduction

While the development of a high performance catalyst may be the Holy Grail for most scientists engaged in catalytic research, providing a molecular level understanding of the chemical events at that reaction centre is tantalising to many. In my previous review in this journal,[1] I investigated the relationships between metal carbonyl cluster complexes and oxide-supported heterogeneous catalysts. One of these, the use of cluster complexes to provide a spectroscopic database for interpreting the spectra of adsorbates in heterogeneous catalysis and surface science, has proved to be of substantial benefit. The other was the attempted synthesis of a uniform array of metal particles on an oxide surface to provide molecular type heterogeneous catalysts. However, in the succeeding years it proved very difficult to maintain low oxidation state cluster complexes under the relatively alien environment of many oxide surfaces (typically silica, alumina and titania). While stabilising interstitial or bridging ligands retarded cluster breakdown, they did not prevent it under catalytic reaction conditions.

It was apparent that a richer vein would be to probe the inorganic chemistry of metals on oxide surfaces, again taking the synthetic strategy from organometallic chemistry, but that would require improved characterisation procedures. In this review, I shall discuss the development of an array of techniques to follow this chemistry. The problem of characterising metal centres on disordered surfaces is not very distinct from that of elucidating solution structures, and we shall also see how similar combinations of spectroscopic techniques can be used to investigate homogeneous catalysts.

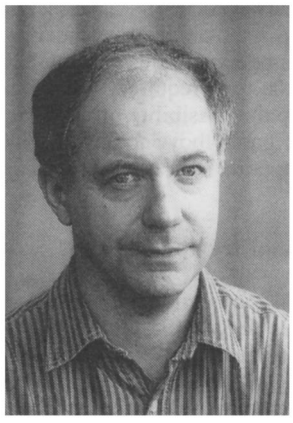

John Evans obtained a BSc in chemistry in 1970 from Imperial College London and then moved to Cambridge to carry out research towards a PhD with Lord Lewis and Brian Johnson. After a year as a postdoctoral assistant at Princeton University with Jack Norton, he returned to Cambridge holding an ICI and then a Royal Society Pickering Research Fellowship. He moved to the University of Southampton in 1976, and was appointed to the Chair of Inorganic Chemistry in 1990.

2 Surface organometallic chemistry (SOMC)

2.1 Surface organometallic chemistry on high surface area oxide surfaces

The parallels between the chemistry of metals on oxide surfaces and in solution have been developed by many groups, with those led by Basset,[2] Gates,[3] Ichikawa,[4] Iwasawa,[5] Marks,[6] Ozin,[7] Schwartz,[8] Ugo and Psaro[9] and Yermokov[10] having been the most prominent. In many instances the chemistry on the oxide surface can be understood using organometallic concepts. An oxide surface might typically provide Brønsted or Lewis base (O^{2-}), Brønsted acid (-OH) and Lewis acid (M^{n+}) sites.

For example, the labile ether ligand in $[RuCl_2(CO)_3(thf)]$ (thf = tetrahydrofuran) can be understood to undergo substitution by a surface silanol of a highly hydroxylated silica surface acting as a Lewis base in this 18-electron Ru^{II} centre (Fig. 1).[11] A more complicated example is found from the reaction of $[OsH_2(CO)_4]$ with the more basic oxide MgO, which has been dehydroxylated at high temperatures (800 °C). The Os^{II} hydride is deprotonated by the strong Brønsted basic oxide ligands to form the 18-electron $[Os^0H(CO)_4]^-$ anion.[12] There is a low frequency ν(CO) absorption in the IR spectrum of this material typical of those caused by a Lewis acid interacting with the carbonyl oxygen (Fig. 2). Under these activation conditions, surface magnesium centres are formed which can fulfil that role. Accordingly, this band is lost on exposure to thf vapour, which preferentially complexes with the cation, so forming a local surface ion pair.

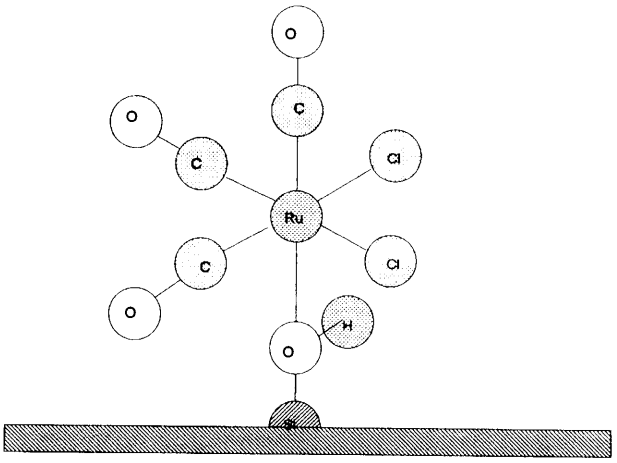

Fig. 1 Proposed reaction product from $[RuCl_2(CO)_3(thf)]$ and silica

Taking a more difficult example, the grafting of $[Rh(\eta^3\text{-}C_3H_5)_3]$ onto silica can be considered to include the electrophilic cleavage of a Rh–allyl bond by a silanol group, leading to the evolution of propene.[13] The surface can then furnish a Lewis base (siloxide) site to coordinate the metal. However, this by itself would provide a 16-electron coordination sphere, the four-electron η^3-allyl anion being displaced by a two-electron siloxide (assuming little π bonding from the siloxide). An

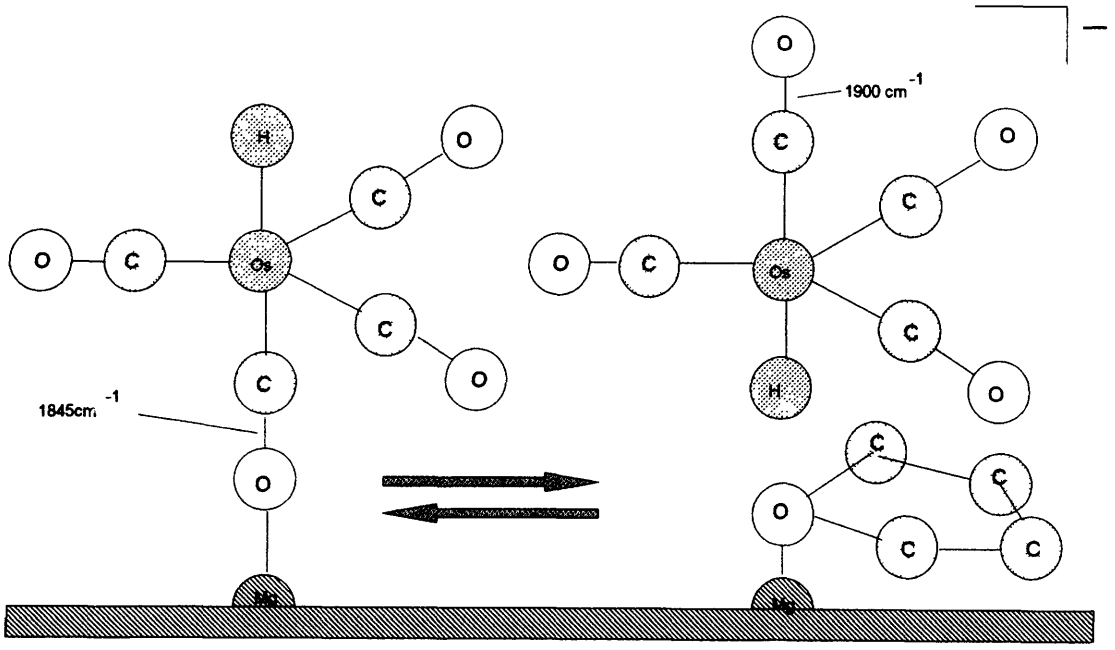

Fig. 2 Proposed surface species from the interaction of $OsH_2(CO)_4$ with MgO (activated at 800 °C) (left) and that on subsequent exposure to thf[12]

alternative structure would involve the interaction of a second oxygen, probably involving a longer M–O bond length from a neutral surface site than that typical of that to an anion Lewis base site. However, observing these is not easy. Mass balance and IR spectroscopic studies provide the surface stoichiometry, and evidence of the η^3-allyl group. We have attempted to locate these distances by using Rh K-edge EXAFS (extended X-ray absorption fine structure).[14] Analysis of this data, however, is consistent with either of these structural proposals since in the presence of the six carbon atoms it is difficult to assess the coordination number of minor light atom shells with any degree of certainty.

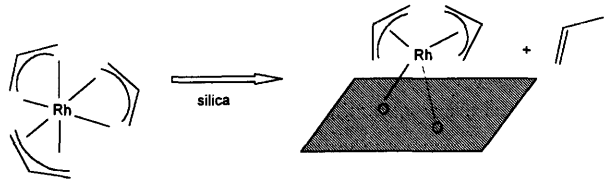

Fig. 3 Proposed surface species from the reaction of $[Rh(\eta^3\text{-}C_3H_5)_3]$ with silica

More promising cases for identifying metal–surface interactions will be provided by centres with lower ancillary ligand coordination spheres. One such centre is the silica supported zirconium hydride formed after the hydrogenation of $[(SIL\text{-}O)Zr(CH_2CMe_3)_3]$. This hydride, which catalyses the cleavage of the C–H and C–C bonds of alkanes, has been characterised by IR, NMR and EXAFS measurements.[15] Three Zr–O bonds were identified at a distance typical of a zirconium(IV)–siloxide group. The zirconium atom, as an eight-electron centre, is highly electron deficient, and this is probably the basis of its high catalytic activity. An additional back-scattering component was also evident, and this suggested that the unsaturation is partially alleviated by a weaker Zr–O interaction (Fig. 4).

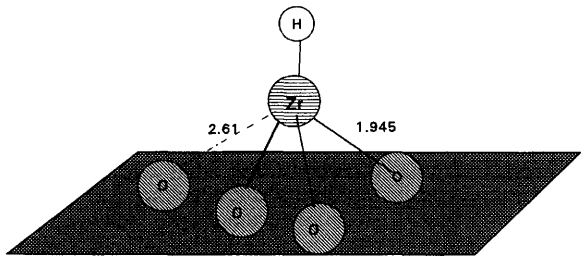

Fig. 4 Proposed structure for a silica supported zirconium hydride catalyst for C–C and C–H activation

One unit which occurs very frequently in oxide-supported rhodium chemistry is the *gem*-dicarbonyl, $Rh(CO)_2$. This was identified very early in the use of IR spectroscopy in conjunction with CO as a chemisorption probe. Its nature was rather contentious, with differing techniques suggesting the rhodium atoms were either isolated (by IR) or on the fringes of two-dimensional rafts (by TEM). This was settled in favour of the former by elegant Rh EXAFS studies by Koningsberger and Prins, which enabled them to probe the metal structure under similar conditions to those of the chemisorption experiments.[16] Not only did they demonstrate that the ancillary ligands were solely oxygen, at distances typical for a Rh^I–O bond, they showed that these centres were formed from the corrosive chemisorption of metal particles. Hence, the use of CO chemisorption to measure rhodium surface area with a presumed surface Rh:CO stoichiometry of 1:1 was flawed. Interestingly, thermolysis of these dicarbonyl units reformed metal particles.

These $Rh(CO)_2$ units have been formed by many groups from molecular precursors, *e.g.* $[Rh(\mu\text{-}Cl)(CO)_2]_2$ and $[Rh_4(\mu\text{-}CO)_3(CO)_9]$ or by reaction of other organometallic centres with CO {*e.g.* $[Rh(\eta^3\text{-}C_3H_5)_2(O\text{-}SIL)]$}. The precursors can either be introduced from solution or by vapour phase deposition (MOCVD). This latter process can be more readily adapted to ultra-high vacuum conditions of the type required by surface science experiments. That opens up the possibility of removing the vagueness implicit in all of the figures above about the oxide binding site since single-crystal supports may be employed.

2.2 A surface organometallic chemistry approach to heterogeneous catalysts

The aim of the approach, derived in conjunction with Professor Hayden in our Department, has been to establish a fundamental understanding of the chemistry associated with oxide-supported transition metal chemistry by using surface science techniques to approach the structural detail now commonplace in molecular organometallic chemistry. This is outlined in Fig. 5. Vapour

phase deposition can be used on to both high-area and single-crystal oxide surfaces and monitored by a library of techniques to follow the chemistry occurring during the interaction of the metal with the oxide and its subsequent reactivity and upon exposure to catalyst substrates, promoters and poisons. Some of the techniques can only readily be applied to one regime or the other, but other linking techniques are required for cross-referencing.

The first extended study with this approach has been on the reaction of $[Rh(\mu\text{-}Cl)(CO)_2]_2$ with titanium dioxide. As might be expected, the $Rh(CO)_2$ units can be formed from MOCVD onto high area titanias. The observation of the symmetric and antisymmetric ν(CO) IR bands is not diagnostic. However, by using $C^{16}O/C^{18}O$ mixtures, the six bands from the three possible isotopomers have been identified.[14] Analysis of the EXAFS data is consistent with the rhodium centres being like that in **1**. A surface rhodium dicarbonyl has also been formed from $[Rh(\eta^3\text{-}C_3H_5)(CO)_2]$, showing that the chlorine is not essential.

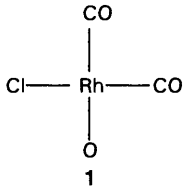

1

Thermolysis of **1** under mild conditions appears to maintain the Rh–Cl bonds, but after heating to 525 K the EXAFS data indicated all the detectable rhodium was in large, ordered *fcc* particles. However, in the chloride-free system, the rhodium particles appeared to be extremely small ($CN_{Rh\text{-}Rh}$ *ca.* 2 and $CN_{Rh\ O}$ *ca.* 0.9) and could be readily disrupted by exposure to CO.[14]

To try to establish the nature of the surface sites adopted by the rhodium on to titania, deposition on to a single-crystal plane of rutile was attempted. The (110) plane is one of the best studied and is the most stable low-index plane of rutile (Fig. 6).[17] This can be prepared as an ordered, stoichiometric surface.

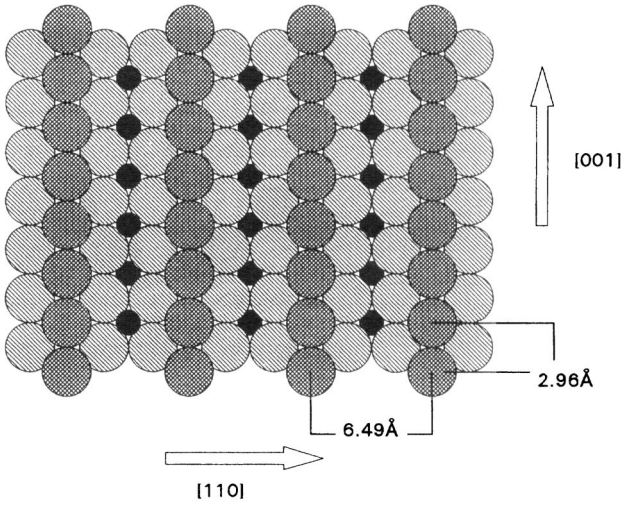

Fig. 6 Structure of the (110) surface of rutile Small circles are Ti, and the cross-hatched shading of the oxygen atoms form the top-most layer

Deposition of $[Rh(\mu\text{-}Cl)(CO)_2]_2$ onto this surface at room temperature generates a chemisorbed species shown by XPS to have very similar Rh binding energy to the precursor, and hence is likely to be rhodium(I).[18] Identifying it as an $Rh(CO)_2$ centre was confirmed by reflection–absorption IR spectroscopy (RAIRS) recorded with an incident angle of 83° and detecting radiation polarised perpendicular to the crystal surface. Under this arrangement the symmetric ν(CO) band appeared as an apparent emission, while the antisymmetric band was a much weaker absorption. This effect will be manifest at near-grazing incidence at a semiconductor surface if these bands are polarised perpendicular and parallel to the surface, respectively. Two possible orientations of the $Rh(CO)_2$ are presented in Fig. 7. In the first of these, (a), the polarisations of the two modes are as observed, while in the second both modes would be polarised at approximately 45° to the surface. Hence the former model is preferred. A remaining difficulty is to establish the fate of the chlorine. XPS shows the rhodium attains a binding energy more like that of surface-bound chlorine after

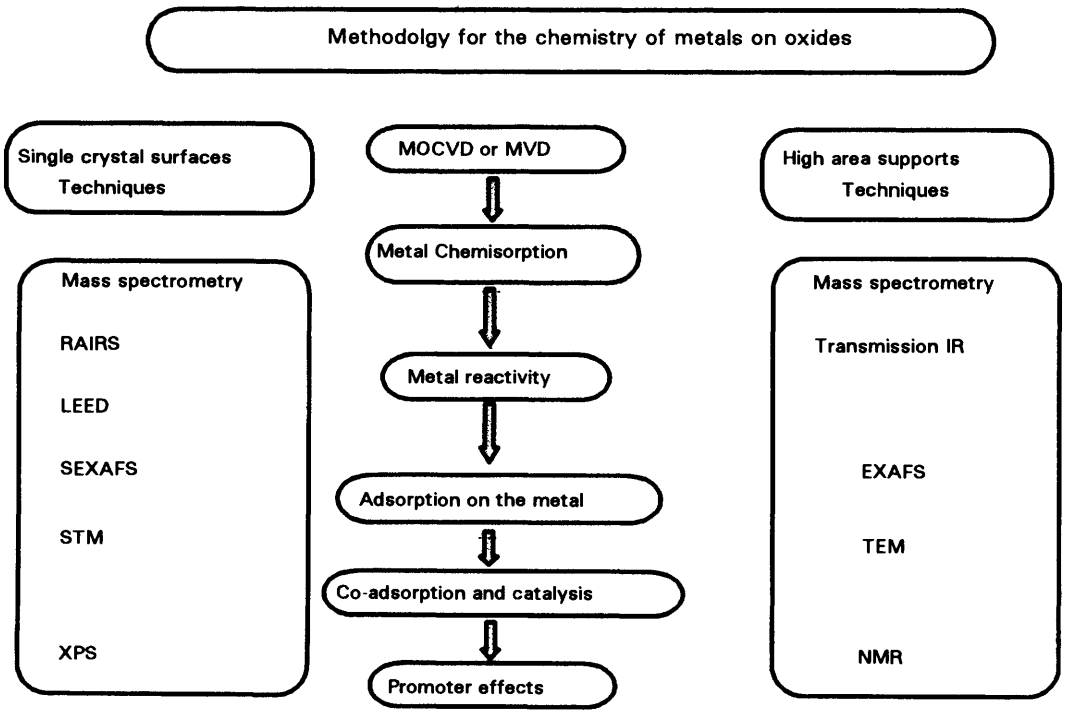

Fig. 5 Methodology for studying the chemistry of transition metals on oxide surfaces

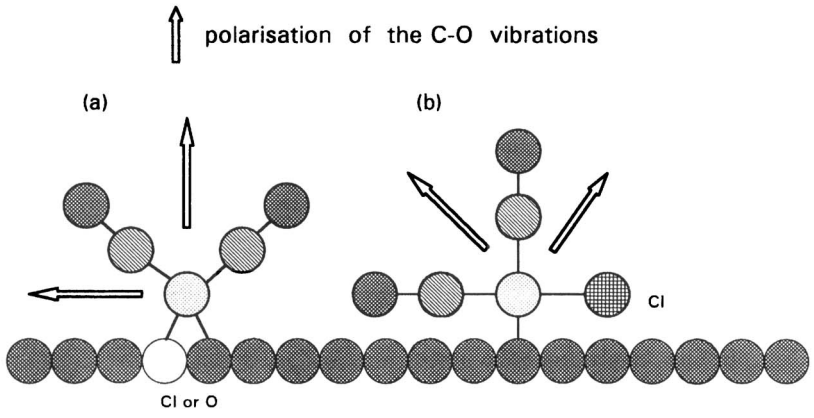

Fig. 7 Surface models for $Rh(CO)_2$ on rutile(110). Model (a) is consistent with the IR observations.

the initial chemisorption, and distinct from that of the Rh-Cl-Rh site. It is not yet clear whether the chlorine is still coordinated to the rhodium or whether a second oxide substitutes it. It is intended that Rh K-edge SEXAFS measurements made on a UHV chamber presently being commissioned will solve this problem. Unfortunately, there is insufficient order in the rhodium carbonyl overlayer to form a LEED pattern.

Thermolysis (800 K) of this species also seems to form large rhodium particles. Under a narrow range of milder conditions the rhodium can be completely decarbonylated but the $Rh(CO)_2$ unit can be partially regenerated. The metal particles which are formed absorb CO in an atypical way for rhodium metal. For comparison, MVD of rhodium was used to form overlayers. These adsorbed CO in a manner very similar to a Rh(111) surface, although the saturation coverages were reduced to *ca* 0.33 and only the terminal (η) CO site could be identified {a μ-CO site is also observed on Rh(111)}. The frequency of the IR band for this site increased with coverage, as is normal. However, the Rh sites formed by thermolysis (resulting from either MOCVD or MVD initially) required about 10^6–10^7 larger exposure of CO to allow observation of the ν(CO) bands in the IR, and then only displayed the frequency for saturation coverage. This implies a rate-determining step before the adsorption of CO on the metal surface. This suppressed CO adsorption behaviour is reminiscent of the SMSI effect (strong metal-to-surface interaction). Various models for this have been proposed, including electronic effects for reduced titanium centres and migration of the oxide surface over the metal. Our evidence confirms the presence of reduced titanium, but also suggests that islands of rhodium sites become available after reaction with CO and the unprotected metal can then rapidly adsorb CO to achieve saturation.[18] Migration of oxygen from titanium dioxide over the rhodium would be consistent with this. It is our intention to characterise the particle growth process in much more detail by *in situ* SEXAFS and STM studies.

In one system, the reaction between $[Rh(\eta^3\text{-}C_3H_5)_3]$ and TiO_2, some differences in behaviour have been observed between experiments carried out on both oxide surface types. In both cases, there is evidence for the reaction of surface hydroxyl groups and the rhodium–allyl bonds, forming $[(Ti\text{-}O)Rh(\eta^3\text{-}C_3H_5)_2]$; this was shown on titania by difference DRIFTS spectra and by O(1s) XPS on hydroxylated rutile (110). Thermolysis of the single-crystal sample under UHV was not clean, but led to decreasing binding energies for both the Rh(3d) and C(1s) XPS peaks, indicative of carbonaceous metal formation.[14] However, related *in situ* experiments using a DRIFTS cell allowed the formation of the $Rh(CO)_2$ unit again. Presumably, the carbonyls emanate from oxidation of the allyl ligands. As yet, we cannot say whether this is due to the higher base pressure in the DRIFTS cell or due to more reactive surface sites in the anatase-rich titania. We aim to distinguish between these using a transmission IR UHV for powdered oxides developed from a design reported by Yates;[19] this will radically reduce the pressure gap between these types of experiments.

Metal vapour deposition onto rutile(110) has also been extended to palladium.[20] An interesting feature of this work is that, on annealing, CO adsorption indicates that the predominant metal plane is Pd(111). At intermediate metal loadings, the LEED pattern from the surface shows reflections due the hexagonal structure of Pd(111) aligned with that of the underlying rectangular net of rutile(110). Consistent with this, STM images show that rectangular Pd clusters are formed which are mutually aligned (and also with a very narrow size distribution). Clearly these two layers are not structurally well matched, and it may be that the interfacial strain limits the potential for metal particle growth.

As yet, these studies have shown some insight into the early stages of the interaction of organometallics with oxide surfaces and begun to show some of their subsequent chemistry. The use of X-ray absorption spectroscopy (XAS) has been an important component in these studies.

3 Spectroscopic characterisation of homogeneous transition metal catalysts

3.1 Scanning XAS studies of homogeneous catalysts

However, the attributes of XAS that make it applicable to disordered heterogeneous catalysts, namely its ability to probe short-range order with element specificity, also make it viable for improving the characterisation of homogeneous catalysts.[21] While NMR and IR spectroscopy can achieve higher resolution in solution and thus be more definitive than in heterogeneous catalysts, there are functional groups which are difficult to identify directly by these techniques alone (*e.g.* M–X bonds when X = Cl, Br and I). Cells can readily be constructed which, by substitution of window material, can be used for IR, UV–VIS and XAS spectroscopies.

For example, the well-known rhodium catalysed methanol carbonylation catalyst[22] can be studied by IR and Rh K-edge XAS in this way.[23] The principal rhodium species in the catalyst system, $[RhI_2(CO)_2]^-$ **2** can readily be identified and the bond-lengths established in solution (Fig. 8). It is known that the initial steps in the reaction are the oxidative addition of CH_3I and then methyl migration. The resulting acetyl complex has been identified by X-ray diffraction as $[Rh(COCH_3)(CO)I_3]_2^{2-}$; the dimer allows the rhodium centres to attain 18 electrons through iodine bridges. In a coordinating solvent, such as methanol, these bridges may be cleaved to a solvated monomer, which may be more important in the catalytic cycle. Rapid-scanning EXAFS studies showed that the dimer can be identified in thf solution at −20 °C, but that it does indeed cleave at 0 °C. The bond lengths obtained on the monomeric acetyl complexes **3** and **4** are fully consistent with the

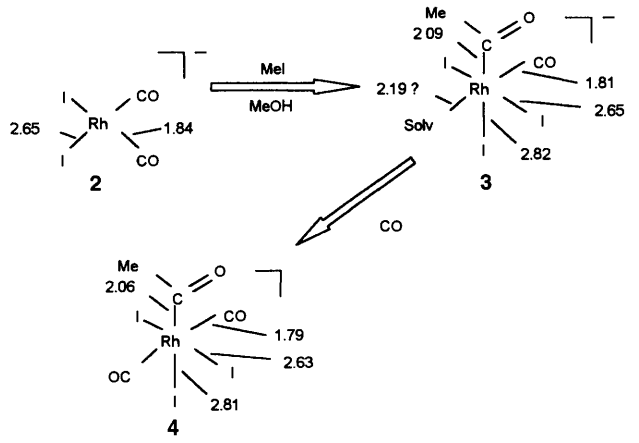

Fig. 8 Interatomic distances established by Rh K-edge EXAFS on the methanol carbonylation catalyst system

stereochemistries shown. The acetyl groups exert a strong *trans*-influence lengthening the Rh–I bond by *ca.* 0.2 Å, and therefore probably labilising it.

Mostly though we have studied the activation of transition metals by main-group metal alkyls. One example of this was the activation of $[Cu(acac)_2]$ by $ZnEt_2$ (1 : 1),[24] which forms an ethanol synthesis catalyst.[25] The adjacency of these two metals in the periodic table allows the fates of both to be followed readily by XAS. The copper was found to form locally ordered *fcc* colloidal particles. Estimates of the particle sizes based on EXAFS coordination numbers alone have substantial error bars. However, for a 1 mM solution in benzene, the particles were sufficiently small that the first coordination number is very sensitive to particle size, estimated as *ca.* 12 Å. The zinc appears to form molecular clusters and so the two metals remain separate in the products.

Among the most utilised systems of this nature (Ziegler–Natta catalysts apart) are those derived from nickel providing a series of catalysts for catenating alkenes.[26] A low temperature solution cell XAS was developed to study these highly reactive solution.[27] Activation of $[Ni(\eta^3\text{-}C_3H_5)Br(PPh_3)]$ by $AlEt_3$ was followed using both the Ni and Br K-edges (Fig. 9). This showed that the Br was predominantly transferred from the nickel to the aluminium (in toluene solution) in the presence of propene, with **6** being a putative structure. Interaction of **5** with $AlEt_3$ at −60 °C was observable in the absence of the alkene, analysis suggesting a Ni-Br-Al unit was present (Ni–Br 2.31; Ni···Al 3.20 Å), as had been previously proposed for the activation process.[26]

A highly active propene oligomerisation catalyst is formed from the activation of $[NiCl_2(PEt_3)_2]$ by $Al_2Me_3Al_3$ or Al_2Et_6.[26] The EXAFS patterns obtained for these systems indicate a

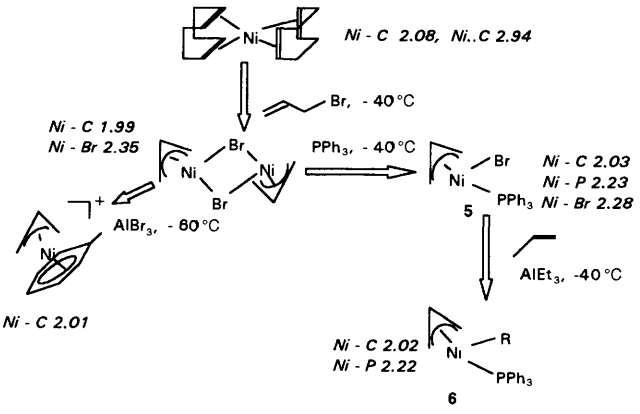

Fig. 9 Results of EXAFS studies of the activation process from $[Ni(\eta^4\text{-}C_8H_{12})_2]$ for alkene oligomerisation catalysts in toluene solution

transmetalation of the alkyl group from aluminium to nickel.[28] The loss of the halide from nickel and its transfer to aluminium is confirmed also for $[NiBr_2(PEt_3)_2]$ by monitoring the bromine K-edge EXAFS data.[29] The EXAFS data at the nickel edge is more complex than that of a simple single coordination shell, and could be fitted satisfactorily by the model shown as **7**.[28] This, however, only represents the mean of a family of related structures although it does indicate an adduct of the aluminium reagent with the nickel complex that is part of the transmetalation process. The oligomerisation catalysis may be terminated and the products isolated by solvolysis with isopropyl alcohol. Under those conditions the nickel reverts cleanly to $[NiX_2(PEt_3)_2]$.

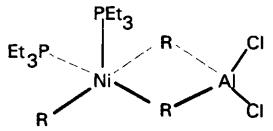

7

These experiments afforded information about the activation processes of these nickel-catalysed reactions, but did not give any insight into the catalytic process. An interesting candidate for this was provided by the mixture of $[Ni(cod)_2]$ (cod = cycloocta-1,5-diene) and the bifunctional ligand $PPh_2CH_2C(CF_3)_2OH$. Not only is this an allylaluminium-free catalyst system, it also was the first instance of direct observation of a nickel hydride by ^1H NMR.[30] This was taken as an indication that the 14-electron species **8** was the active component. This complex requires the oxidative addition of the hydroxyl group; without the electron-withdrawing CF_3 groups this is extremely difficult.

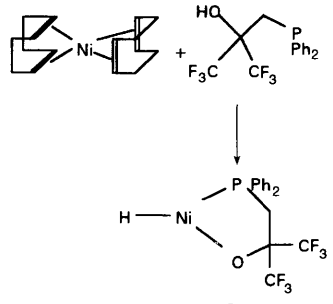

8

However, the multiplicity of the hydride resonance (apparent triplet) is not consistent with the structure **8**. It was found that the intensity of this resonance was maximised with a Ni : ligand ratio of 1 : 2, and the structure **9** (Fig. 10) was established by a combination of ^{31}P NMR and Ni K-edge EXAFS.[31] Essentially, this is a version of the highly unsaturated transient **8** trapped by the second, monodentate phosphine. On exposure to ethene or propene alkene insertion reactions occur at the nickel hydride bond with the remainder of the coordination sphere intact in the predominant species. On warming, β-hydride elimination regenerates the hydride **9**.

In this example we have observed the apparent sequences of an alkene oligomerisation process: alkene insertion into Ni–H and then Ni–C bonds, followed by the β-hydride elimination to remove a higher alkene from the coordination sphere. However, the reaction rate is maximised not at the Ni : L ratio of 1 : 2 but at an equimolar ratio. This is consistent with phosphine loss from **9** being kinetically important in the oligomerisation process. So it is quite possible that a three-coordinate species like **8** is indeed key to the reaction mechanism, and that our experiments have probed the resting form of the catalyst.

The structural motif of a unicharged bidentate ligand is also provided by β-diketonates, and for some time it has been known that activation of $[Ni(acac)_2]_3$ (acac = pentane-2,4-dionato) by

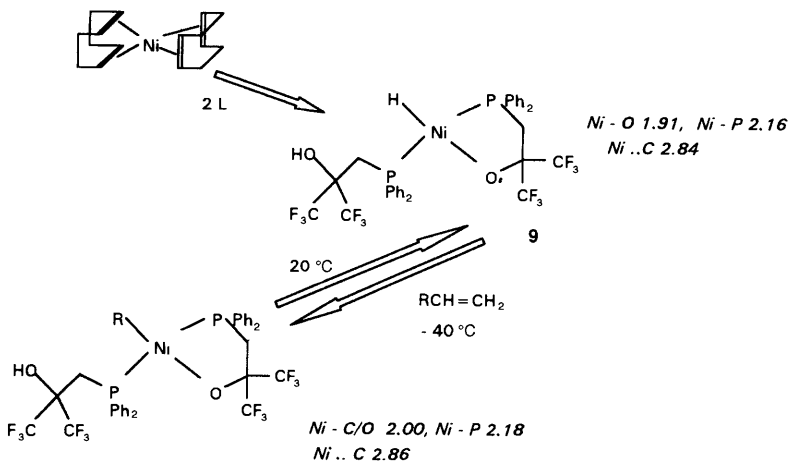

Fig. 10 Results of EXAFS and NMR studies of the activation process from $[Ni(\eta^4\text{-}C_8H_{12})_2]$ and $PPh_2CH_2C(CF_3)_2OH$ for alkene oligomerisation catalysis

$AlEt_2(OEt)$ affords a hex-1-ene dimerisation catalyst in toluene solution.[32] Interestingly, this system formed a temperature dependent equilibrium, with the green, paramagnetic precursor dominating at low temperatures (*e.g.* −70 °C). The nature of the active yellow–brown form was not established. By monitoring this reaction at various temperatures by Ni K-edge EXAFS, we gained evidence for a structure consistent with that shown as **11** in Fig. 11.[33] The alkene could be readily displaced by a phosphine to afford complex **12**, which has a similar coordination sphere to **10** in the system derived from the bifunctional phosphine. It is therefore plausible that a derivative of **11** may well play a key role in that catalytic cycle also.

So these results lead to a generalised catalytic cycle for alkene dimerisation as shown in Fig. 12. Extensions of this with repeated alkene insertions into Ni–C bonds will lead to oligomer and polymers. This scheme has close parallels with the cationic nickel- and palladium-diazabutadiene systems recently reported by Brookhart *et. al.*[34] and the intermediates follow the results of density functional calculations by Ziegler and coworkers.[35] Versions of three of the species in this scheme, **13**, **14** and **15** have been observed by EXAFS. Two of these **13** and **14** are stabilised forms of the catalyst precursor or an intermediate in the cycle and are therefore external to the cycle. Our proposal for a complex comprising [Ni(R)(alkene)(acac)] **11** corresponds to species **15** within the catalytic cycle, and is closely related to some of the catalyst precursors with diazabutadienes as auxiliary ligands.[34] However, the DFT calculations of Ziegler suggest that the agostic hydrogen interactions in **17** outweigh the π-bonding stabilisation in the nickel–hydride–ethene complex, and also the γ-H interaction in **16** will render it more stable than **15** by over 40 kJ mol^{-1}.[35] More stable again is predicted to be the β-agostic species **18**, by an additional 40 kJ mol^{-1} and might therefore be expected to predominate in solution. In **18**, the two Ni–C distances were calculated as Ni–C_α = 1.86 and Ni–C_β as 2.06 Å, while the EXAFS data for the species assigned as **11** refined as a shell of 3.1(4) carbon atoms with Ni–C = 2.025(4) Å. So differentiation between these structures is dependent upon the estimation of the coordination numbers. While this is not the most precise aspect of EXAFS analysis, it must be noted that a structure like that of **18** requires an error of 3σ. So the initial proposal of the alkyl–alkene complex **11** provides a better, but not definitive, account for experimental observations. Therefore trying to reconcile this with the results of the DFT calculations is difficult, but we must note the longer alkyl groups in both the β-diketonate and hydrocarbon ligands used in the experiments. However, the results of these DFT calculations were used to suggest that the Ni–H NMR resonance observed by Keim *et al.*[30] was due to an intermediate of the type $[NiH(alkene)_2(E\text{--}E)]$[35] which is inconsistent with our EXAFS and NMR results.[31]

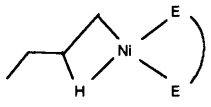

18

3.2 Energy dispersive EXAFS (EDE)

Even in a rapid scanning mode, the time required to record an analysable length of EXAFS data (500 eV) is of the order of minutes, while, for a dilute sample, several hours might be taken to obtain optimised data. So such experiments can only be used to investigate the structures of the dominant species stable for those time periods. Clearly, to be able to observe some of the intermediates in a catalytic reaction, these must be generated in high proportion and identified prior to their decay. An

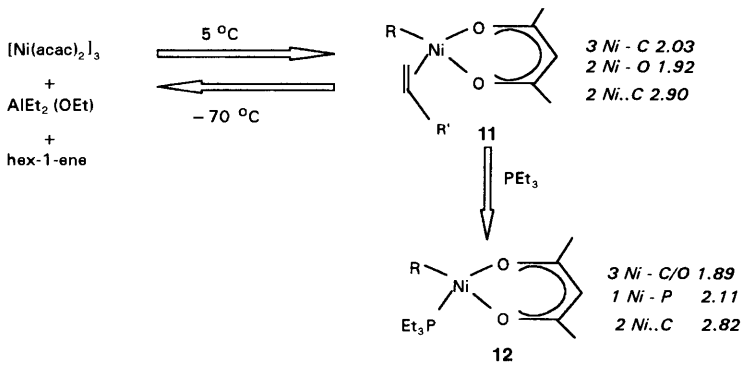

Fig. 11 Results of EXAFS studies of the activation process from $[Ni(acac)_2]_3$ and $AlEt_2(OEt)$ for hexane dimerisation catalysis

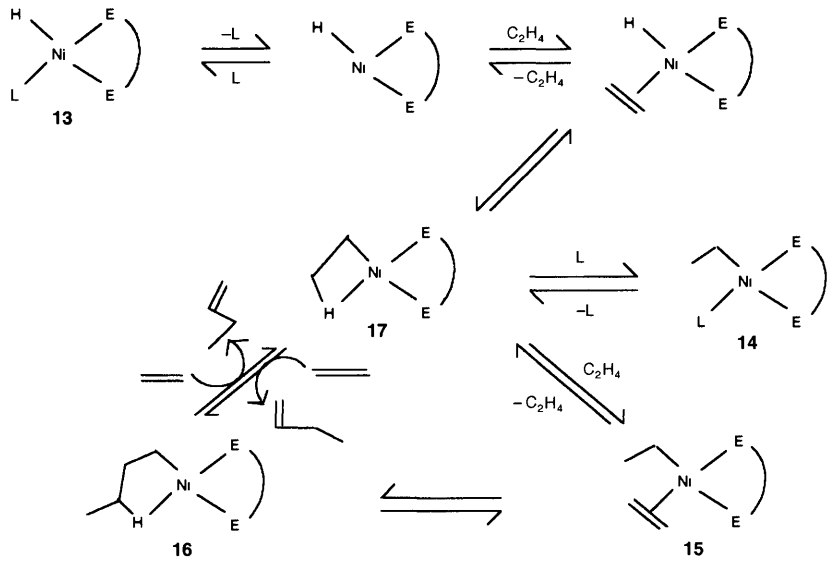

Fig. 12 Generalised cycle for alkene dimerisation by nickel catalysts with a bidentate auxiliary ligand

alternative method of acquiring X-ray absorption spectra is to expose the sample to the spectral range and to disperse this across a multi-element detector. This can be achieved by taking the white radiation from a dipole or wiggler magnet on a synchrotron source (as at the SRS at Daresbury Laboratory) or by tuning a harmonic of an undulator to cover the spectral range. The band spread is then obtained by a curved crystal monochromator, which can be in either a Bragg (reflection) or Laue (transmission) geometry (Fig. 13). A slightly different incident angle is experienced at different points on the monochromator, and the spread of wavelengths so formed is focused onto the sample whence it defocuses onto the detector, typically either a photodiode array (PDA) or a CCD camera.

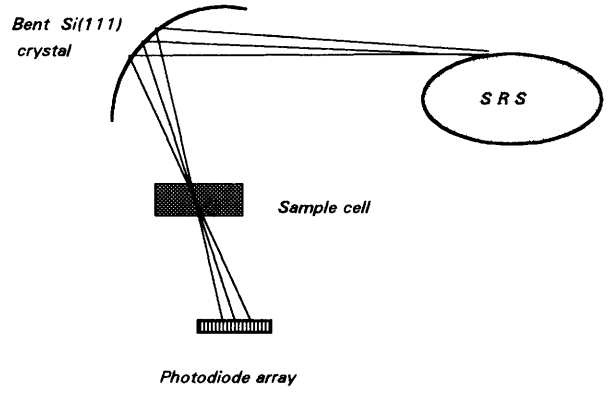

Fig. 13 Schematic layout of an energy dispersive EXAFS (EDE) experiment with a Bragg-geometry monochromator. (The bend and Bragg angle are exaggerated to emphasise the ray pathways of different X-ray energies).

The experiment gains temporally by removing the need to move any part of the optical system during the data acquisition and by the synchronous acquisition of all data points (the multiplex advantage). The difficulties arise from the needs to attain very sensitive, high output linearity X-ray stable detectors and a high optical purity and stability. The geometry constrains the detection to a transmission mode, and so the technique of choice for very dilute samples, fluorescence, cannot be employed. Recent advances in these technologies indicated that it should be possible to acquire spectra in times of the order of seconds, and a likely goal of milliseconds was feasible. So experiments were carried with modified versions of the variable temperature cells described previously,[27] fitted with a pair of syringe drivers to allow continuous flow or stopped flow. Depending on the volume of the cell employed, perfect plug flow would give residence times of 1–10 s, although the real mixing times were somewhat longer.[33] Very recently an ambient temperature cell with a mixing time of 5 ms has also been employed.[29]

An example of EXAFS data from one of these experiments is shown in Fig. 14.[33] The total acquisition time for this spectrum was 2 s on a solution 70 mM in nickel. This spectrum, of the reaction of $[Ni(acac)_2]_3$, hex-1-ene and $AlEt_2(OEt)$, is intermediate between that of $[Ni(acac)_2]_3$ and that of the activated solution, assigned to complex **11**. The feature evident in the Fourier transform near 3 Å is best fitted as the Ni···Ni distances in a retained trimer. It is suggested that the trimer undergoes a transmetalation of the alkyl group from the aluminium reagent at the terminal nickel centres prior to dissociation into the monomeric units of the activated solution. The behaviour of the

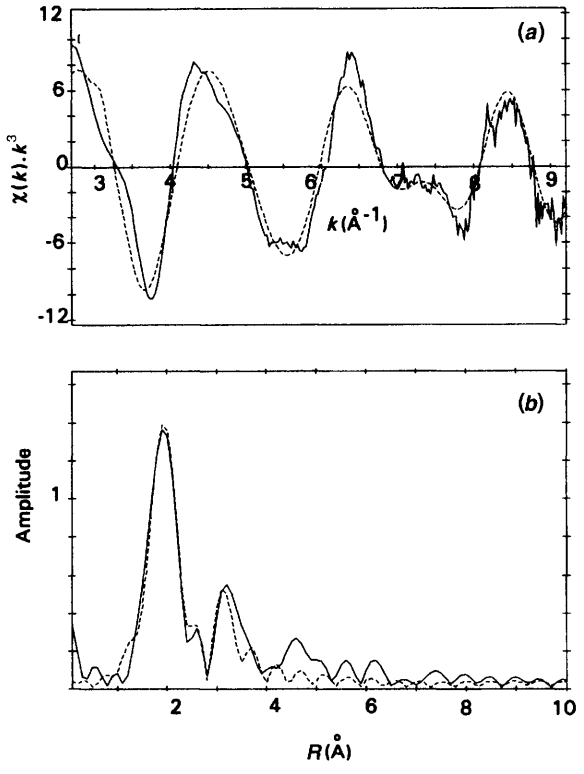

Fig. 14 Ni K-edge EXAFS analysis of the $Ni(acac)_2$, $AlEt_2(OEt)$ Ni : Al = 1 : 2) and hex-1-ene (Ni : hexene = 1 : 20) solution after 4.75 min at 0 °C. Average of 100 scans of 20 ms. (*a*) EXAFS and (*b*) Fourier transform with (—) experimental and (---) calculated curves.

UV–VIS spectra of such solutions also suggests that there is a short-lived species.

These experiments have demonstrated the viability of EDE for probing the structures of transients during organometallic reactions in the liquid phase. As is evident from section 2.2 of this review, similar experiments might be carried out on supported complexes. Fig. 15 shows a stacked plot of the results of monitoring the reaction of $Rh(CO)_2$/titania with hydrogen by Rh K-edge EDE.[14] Such an experiment is not currently possible at the SRS. The penetrating nature of the X-radiation at these energies (*ca.* 24 keV) means that there is a spread of effective X-ray source positions through the crystal for a given energy which then diffuses over several elements of the detector array, so reducing the spectral resolution very markedly. This can be circumvented by using a thin single-crystal wafer as the monochromator set up in a transmission (Laue) geometry {carried out using a 100 μ thick Si(111) crystal on ID24 of the ESRF}.

Energy dispersive Rh K-edge EXAFS (EDE) experiments were performed on the thermolysis and hydrogenation of $Rh^I(CO)_2/TiO_2$ samples with *ca.* 3 mass% rhodium. EXAFS data for up to 10 $Å^{-1}$ could be acquired with typically 250 × 15 ms scans (*ca.* 6 s acquisition time). These have yet to receive detailed analysis, but the following observations are apparent from qualitative treatments on stacked plots of raw data (*e.g.* Fig. 15). When $Rh^I(CO)_2/TiO_2$ was heated *in vacuo* (10^{-5} mbar) as the sample temperature was ramped from ambient temperature to 300 °C, it was apparent that there was a smooth transformation of $Rh(CO)_2$ into metallic rhodium above 220 °C, with no identifiable intermediate. Alternatively, when the sample was heated under a flow of H_2 within the vacuum system as the temperature was ramped, reduction by H_2 to rhodium particles occurred most rapidly in a period of 1 minute as the temperature passed through the 80–90 °C range. In combination with isothermal experiments carried out near this temperature region, these results suggest that the reduction may be autocatalytic. This might arise if the dissociative chemisorption of hydrogen, possibly the rate-determining step in the particle formation, is more rapid on small rhodium particles than at the $Rh(CO)_2$ centres.

4 Concluding comments

The two main aims of this research have been to improve the characterisation of homogeneous transition metal catalysts and to raise the plane of understanding of oxide-supported metal catalysts to that attainable in solution. These have so far been met imperfectly but further progress is in prospect. The current developments in X-ray absorption spectroscopy indicate that *in situ* studies of intermediates catalysed reactions are viable, once these have been generated by stopped flow (liquid phase) or pulsed-flow (gas-solid reactors). In the next year or two, structural information of species stable only on a millisecond timescale should be achievable. A more distant horizon is provided by photochemically generated transients, requiring sub μs data acquisition. But the ability to establish structures in disordered phases of such primary species is enticing. Potentially with stable, third generation synchrotron sources in a single bunch mode it should be possible to reconstitute analysable EXAFS data from a set on time-slices obtained at different X-ray energies.

Deriving molecular-level descriptions of the chemistry of oxide-supported metals is still proving to be very challenging. However, we have shown that combining studies on powdered and single crystal oxide surfaces can offer considerable insight the chemistry underlying heterogeneous catalysis. Further *in situ* techniques—STM and SEXAFS—for studying the structures on single-crystal surfaces are currently being developed and we have every prospect of visualising this chemistry with greater precision in the coming months.

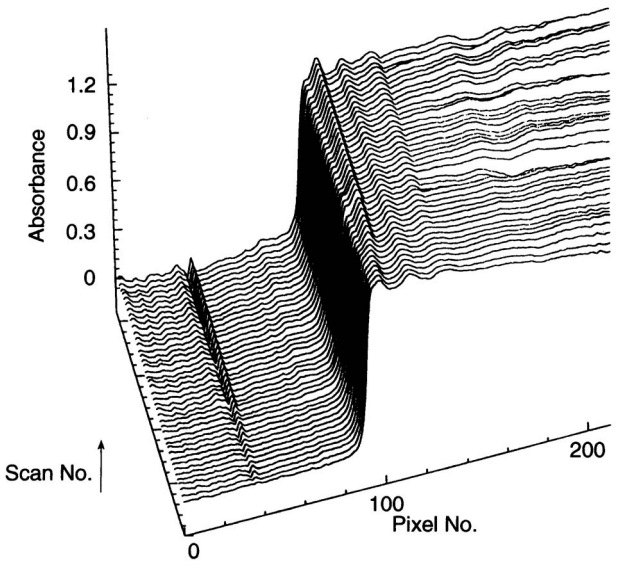

Fig. 15 Stacked plot of Rh K-edge EDE of the reaction of $Rh(CO)_2$/titania with hydrogen. Sample heated from room temperature to 100 °C and then maintained at that temperature.

5 Acknowledgements

I wish to thank all my coworkers cited in the references below for making this research so enjoyable. I am especially grateful to Norman Binsted, Judith Corker, Brian Hayden and Tony Masters (University of Sydney) for making most of this all possible. The debt we owe to the staff of the Daresbury Laboratory and ESRF is a great one, especially the station scientists most involved with these experiments—Bob Bilsborrow, Gerd van Dorrsen, Andy Dent and Michael Hagelstein. The financial support of the SERC, the EPSRC, the University of Southampton and the BP group is also very gratefully acknowledged.

6 References

1 J. Evans, *Chem. Soc. Rev.*, 1981, **10**, 181.
2 J. M. Basset, J. P. Candy, A. Choplin, B. Didillon, F. Quignard and A. Theolier, in *Perspectives in Catalysis*, ed. J. M. Thomas and K. I. Zamaraev, Blackwell, Oxford, 1992, p. 125.
3 B. C. Gates, in *Metal Clusters*, ed. M. Moskovits, Wiley, New York, 1986, p. 283.
4 M. Ichikawa, *Adv. Catal.*, 1992, **38**, 283.
5 Y. Iwasawa, *Adv. Catal.*, 1987, **35**, 187.
6 T. J. Marks, *Acc. Chem. Res.*, 1992, **25**, 57.
7 G. Ozin, S. Özkar and R. A. Prokopowicz, *Acc. Chem. Res.*, 1992, **25**, 553.
8 J. Schwartz, *Acc. Chem. Res.*, 1985, **18**, 302.
9 R. Psaro and R. Ugo, in *Metal Clusters in Catalysis*, ed. B. C. Gates, L. Guczi and H. Knözinger, Elsevier, Amsterdam, 1987, p. 427.
10 Yu. I. Yermakov and V. Zakharov, *Adv. Catal.*, 1975, **24**, 173.
11 J. J. Burmeister III and B. E. Hanson, *Inorg. Chem.*, 1990, **29**, 4055.
12 H. H. Lamb and B. C. Gates, *J. Am. Chem. Soc.*, 1986, **108**, 81.
13 M. D. Ward, T. V. Harris and J. Schwartz, *J. Chem. Soc., Chem. Commun.*, 1980, 357.
14 A. J. Dent, J. Evans, M. Hagelstein, B. E. Hayden, J. F. W. Mosselmans, A. Murray, C. J. Rudkin and N. A. Williams, unpublished results.
15 J. M. Corker, F. Lefebvre, C. Lécuyer, V. Dufaud, F. Quignard, A. Choplin, J. Evans and J.-M. Basset, *Science*, 1996, **271**, 966.
16 H. F. J. van't Blink, J. B. A. C. van Zon, T. Huizinga, D. C. Koningsberger and R. Prins, *J. Am. Chem. Soc.*, 1985, **107**, 5742.
17 *The Surface Science of Metal Oxides*, V. E. Heinrich and P. A. Cox, Cambridge University Press, Cambridge, 1994.
18 J. Evans, B. E. Hayden, J. F. W. Mosselmans and A. Murray, *J. Am. Chem. Soc.*, 1992, **114**, 6912; *Surf. Sci.*, 1994, **301**, 61.
19 R. R. Cavanagh and J. T. Yates, Jr., *J. Chem. Phys.*, 1981, **75**, 1551.
20 J. Evans, B. E. Hayden and G. Lu, *Surf. Sci.*, 1996, **360**, 61.

21 *X-ray Absorption: Principles, Applications, Techniques of EXAFS, SEXAFS and XANES*, ed. D. C. Koningsberger and R. Prins, Wiley, New York, 1988.
22 D. Forster, *Adv. Organomet. Chem.*, 1979, **17**, 255.
23 N. A. Cruise and J. Evans, *J. Chem. Soc., Dalton Trans.*, 1995, 3089.
24 J. M. Corker and J. Evans, *J. Chem. Soc., Chem. Commun.*, 1994, 1027.
25 M. Simon, A. Mortreuz and F. Petit, *J. Chem. Soc., Chem. Commun.*, 1988, 1445.
26 *The Organic Chemistry of Nickel*, P. W. Jolly and G. Wilke, Academic Press, New York, 1975, vol. 2; W. Keim, *Angew. Chem., Int. Ed. Engl.*, 1990, **29**, 235; G. Wilke, *Angew. Chem., Int. Ed. Engl.*, 1988, **27**, 206.
27 P. Andrews, J. M. Corker, J. Evans and M. Webster, *J. Chem. Soc., Dalton Trans.*, 1994, 1337.
28 J. M. Corker and J. Evans, *J. Chem. Soc., Chem. Commun.*, 1991, 1104.
29 J. M. Corker, A. J. Dent, J. Evans, M. Hagelstein and V. L. Kambhampati, *J. Physique (C)*, in the press.
30 U. Müller, W. Keim, C. Kruger and P. Betz, *Angew. Chem., Int. Ed. Engl.*, 1989, **28**, 1011.
31 P. Andrews and J. Evans, *J. Chem. Soc., Chem. Commun.*, 1993, 1246.
32 J. R. Jones and T. J. Symes, *J. Chem. Soc. C*, 1971, 1124.
33 D. Bogg, M. Conyngham, J. M. Corker, A. J. Dent, J. Evans, R. C. Farrow, V. L. Kambhampati, A. F. Masters, D. Niles McLeod and C. A. Ramsdale, *Chem. Commun.*, 1996, 647.
34 L. K. Johnson, C. M. Killian and M. Brookhart, *J. Am. Chem. Soc.*, 1995, **117**, 6414.
35 L. Fan, A. Krzywicki, A. Somogyvari and T. Ziegler, *Inorg. Chem.*, 1994, **33**, 5287; 1996, **35**, 4003.

Received, 2nd September 1996
Accepted 27th September 1996